An examination of the physical variability around the Pribilof Islands in 2004

P.J. Stabeno [a,*], N. Kachel [b], C. Mordy [b], D. Righi [b], S. Salo [a]

[a] NOAA/Pacific Marine Environmental Laboratory, 7600 Sand Point Way NE, Seattle, WA 98115-6349, USA
[b] Joint Institute for the Study of the Atmosphere and Ocean, Box 354235, University of Washington, Seattle, WA 98195, USA

ARTICLE INFO

ABSTRACT

The Pribilof Islands form a unique ecosystem. An anti-cyclonic oceanic flow exists around the islands. Nutrients are introduced into this circulation from two sources: (1) the flow along the 100-m isobath with intrusions of nutrient-rich water in Pribilof Canyon, and (2) the westward transport and vertical mixing of middle-shelf water, which contains nutrient-rich bottom water. Enhanced tidal mixing around the Pribilofs introduces this deeper, nutrient-rich water into the euphotic zone and thus supports prolonged production around the islands. Further, the middle-shelf water that is advected into the region causes the upper 50 m of the water column around the islands to freshen throughout the summer. This enhances the frontal structure and strengthens the baroclinic flow along the 100-m isobath. The strengthening of the frontal structure can moderate ecosystem productivity by limiting the intrusion of slope water rich in nutrients and oceanic copepods.

Published by Elsevier Ltd.

1. Introduction

The Pribilof Islands (Fig. 1) lie in the Bering Sea, a semi-enclosed basin separated from the North Pacific by the Aleutian Arc and from the Arctic Ocean by Bering Strait (Stabeno et al., 1999a). Almost half of the sea is comprised of a broad (>500 km), shallow eastern shelf, with the remainder consisting of a moderately deep basin ($<\sim4000$ m) and a narrow western shelf. This sea supports a rich and varied ecosystem including vast populations of migratory birds, marine mammals and fish (Stabeno et al., 2006). The islands support communities of Aleuts that depend on the sea for food and economic survival. Changes in climate at decadal or longer time scales could have profound consequences for both the ecosystem and economy of this productive archipelago. To be able to anticipate the effect of such changes, an understanding of the mechanisms that control the biological productivity is necessary.

The circulation in the southeastern corner of the Bering Sea basin (Fig. 1) is dominated by the Aleutian North Slope Current (ANSC) and Bering Slope Current (BSC) (Stabeno et al., 1999a). The ANSC flows northeastward along the north slope of the Aleutian Islands (Fig. 1) and turns northwestward at the shelf break to form the BSC (Stabeno et al., 2007a). Water flowing through the Aleutian Passes contributes salt, heat and nutrients to the ANSC. The water in the upper 100–200 m tends to be nutrient rich because of energetic mixing that occurs in the passes (Mordy

et al., 2005; Stabeno et al., 2005). Instabilities in the BSC (Stabeno and van Meurs, 1999; Mizobata et al., 2008) and interaction of the slope flow with topography, such as Pribilof and Bering Canyons (Schumacher and Stabeno, 1998), can both result in the intrusion of nutrient-rich water onto the shelf. The flow over the southern shelf is weakly northward along the 100-m isobath and with anti-cyclonic circulation around the Pribilof Islands (Fig. 1).

Hydrography and currents differentiate the cross-shelf oceanographic structure of the southeastern shelf into three domains with distinct characteristics (Coachman, 1986; Schumacher and Stabeno, 1998; Kachel et al., 2002). A combination of tidal currents and winds results in a weakly stratified or well-mixed coastal domain ($z<\sim50$ m). Over the middle shelf domain ($\sim50<z<\sim100$ m), tides and winds during summer cannot stir the entire water column, resulting in a sharp, two-layered system. The outer-shelf domain ($\sim100<z<\sim180$ m) has a three-layered structure, with well-mixed surface and bottom layers separated by a layer of changing temperature and salinity. Transition zones separate the three domains. The inner front separates the coastal domain from the middle domain; the middle transition separates the middle domain from the outer domain; and the shelf break front separates the outer domain from the slope water (Schumacher and Stabeno, 1998; Stabeno et al., 1999b; Kachel et al., 2002).

The Pribilof Islands sit in the vicinity of the middle transition. Because of the shoaling bathymetry around the islands and their proximity to the shelf break, this region has characteristics that are unique on the shelf. Sullivan et al. (2008) have proposed that this domain be referred to as the "Pribilof Domain". Its uniqueness is a result of its geographic location. Except for the Pribilof Islands, it is only at the northern and southern extremes of the shelf break

* Corresponding author. Tel.: +1 206 526 6453; fax: +1 206 526 6485.
E-mail address: Phyllis.Stabeno@noaa.gov (P.J. Stabeno).
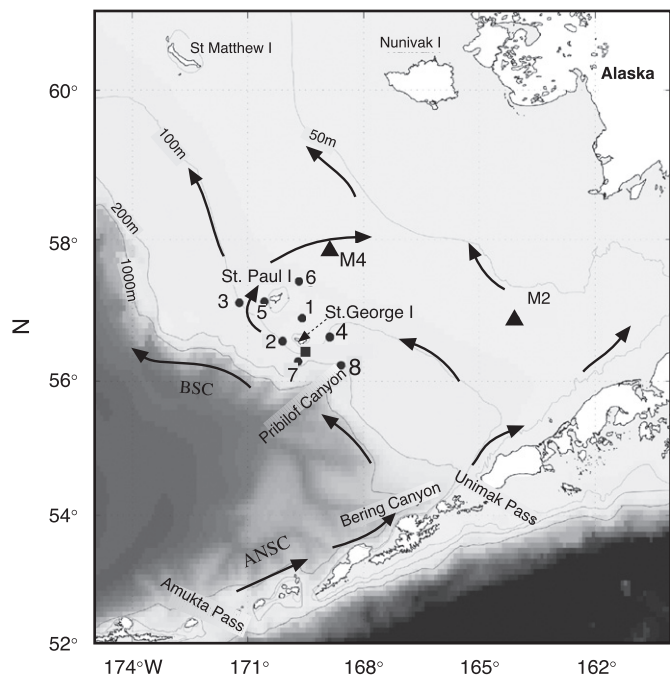
Fig. 1. Southeastern Bering Sea with major currents, locations of Pribilof moorings (1–8) and two long-term biophysical moorings along the 70-m isobath (M2 and M4). The square indicates the location of the ADCP mooring in 1997–1998. The two major currents in the basin are the eastward flowing Aleutian North Slope Current (ANSC) and the northwestward flowing Bering Slope Current (BSC). The weaker flow on the southeastern shelf is also indicated.

that close proximity between the basin and coastal domains occurs (Fig. 1).

The Pribilof Islands consist of four separate islands: St. Paul Island, St. George Island, Walrus Island and Otter Island. St. Paul and St. George Islands comprise over 97% of the total land area. They are separated by ~90 km, with St. George Island found farther south and closer to the shelf break than St. Paul Island. Walrus Island lies slightly east of St. Paul Island, and Otter Island lies south of St. Paul Island.

From 26 July to 20 August 2004, an interdisciplinary research cruise was conducted to examine the ecological processes that affect the productivity of Pribilof Islands' waters and the ability of this ecosystem to support zooplankton and juvenile fish, as well as the seabirds and marine mammals that consume them. This study examined physical processes, nutrient availability, primary production, zooplankton community structure and biomass, and the diets of seabirds with a goal to understand how the ecosystem would respond to climate variability.

This article focuses on the physical environment and the impact of bottom-up processes on primary production. It utilizes data from eight moorings that were deployed in the vicinity of the Pribilof Islands, two long-term biophysical moorings deployed over the middle shelf, satellite-tracked drifters, ship-board measurements and satellite images. We begin with a description of the winds and ice extent over the eastern shelf in 2004, and how ice impacted the spatial and temporal patterns of chlorophyll. We then use satellite-tracked drifters to examine the long-term mean flow around the islands compared to the flow in 2004. Next, we use data from the moorings to examine mechanisms that control flow onto the shelf and the balance between middle-shelf water and the outer shelf/slope waters. We use a hydrographic model to examine how mechanisms, particularly tides, are important to this ecosystem. Finally, we present chlorophyll patterns and relate them to physical

mechanisms that are important in the bottom-up control of this ecosystem.

2. Methods

2.1. Hydrography and nutrients

Conductivity–temperature–depth (CTD) data were obtained using a Seabird SBE9plus system with dual temperature and salinity sensors. The data were recorded on downcasts, which had descent rates of 15–30 m min^{-1}. Salinity calibrations were provided by water samples taken during most of the casts. These data indicated instrument accuracy better than 0.01 psu. Data were routinely examined to remove spurious values. Water samples were collected for analysis of nutrient concentrations at 0, 10, 20, 30, 50 m and near the bottom of each CTD cast. Nutrient samples were collected using polyethylene scintillation vials and caps, pre-washed with dilute HCl and triple rinsed with sample water. Samples were stored upright in a refrigerator until they were processed, normally within 1–2 h, using an on-board Apkem RFA Model 300 automated nutrient analyzer (Whitledge et al., 1981). These *in situ* measurements also provided quality control for the time series collected by the moored nutrient sampler.

2.2. Meteorology

Weather observations are made routinely at the St. Paul airport on the southern part of the island at an elevation of 7 m; maximum elevation on the island is 180 m. Since the Pribilof Islands are low-lying islands, they cause little or no orographic effects on wind fields. While historically the frequency of weather reports was variable, data are now collected hourly.

Simulated winds (e.g., NCEP) provide a good replication of the winds in the Bering Sea (Ladd and Bond, 2002). These fields are used herein to explore spatial variability of the winds and their impact on oceanographic features through Regional Ocean Modeling System (discussed in Section 2.5).

2.3. Moorings

Eight moorings were deployed near the Pribilof Islands from the NOAA Ship *Miller Freeman* on April 30–May 1, 2004 (Fig. 1). Six of the moorings were recovered between September 30 and October 2, 2004. The releases on the other two moorings (P2 and P7) failed to respond, and, because of adverse weather, the ship could not remain on site. Mooring P7 was successfully recovered April 30, 2005. P2 was found on May 5, 2005, but unfortunately it had been dragged ~10 km by a fishing boat and was badly damaged; only the bottom three instruments were recovered. Examination of the three temperature time series from P2 indicated that the mooring was dragged in late December. Depths of the instruments from all the moorings are presented in Table 1. All instruments were calibrated before and after deployment. Each of the deployments (recoveries) was followed (preceded) by a CTD cast and a bongo tow.

Biophysical moorings have been maintained at two sites, M2 (since 1995) and M4 (since 1999), along the 70-m isobath of the southeastern Bering Sea shelf (Fig. 1). During the summer of 2004, a surface mooring was deployed at M2 and a taut wire/chain subsurface mooring was deployed at M4; during winter both sites contained subsurface moorings. Each mooring was instrumented to measure temperature, salinity, nutrients and fluorescence; the surface mooring also measured meteorological variables. Next to each biophysical mooring, a bottom-mounted, upward-looking

Table 1
The positions of and instruments on eight moorings around the Pribilof Islands

Mooring	N latitude W longitude	Depth (m)	Temperature (°C)	Salinity (m)	Fluor. (m)	Currents	Nitrate (m)
P1	56.90° 169.59°	69	12,13,18,23, 28,33,43,57	12,13,57	12	ADCP 300 kHz	
P2	56.58° 170.10°	100	57,76				92
P3	57.12° 171.22°	101	12,13,22,32, 42,57,76,94	12,13,94	12	ADCP 300 kHz	91
P4	56.63° 168.88°	102	12,13,22,32, 42,57,76,94	12,13,94	12	ADCP 300 kHz	
P5	57.13° 170.57°	68	12,13,22,42, 56	12,13,56	12	ADCP 300 kHz	
P6	57.42° 169.67°	68	11,12,21,31, 41,56	11,12,56	11		
P7	56.29° 169.70°	200	188	188		RCM-9 191 m	
P8	56.23° 168.58°	199	186	186		RCM-9 189 m	

Both acoustic Doppler current profilers (ADCP) and single-point current meters (RCM-9) were located within 10 m of the bottom. The ADCPs collected data in 5-m bins. Gaps in the table indicate no data either due to loss or failure of the instrument.

acoustic Doppler current profiler (ADCP) was deployed. In general, temperature on M2 and M4 was measured every 3–4 m in the upper 35 m and at 5–8 m intervals below that. Details of the mooring designs and instrumentation can be found in Stabeno et al. (1998, 2001, 2007b).

A mooring was deployed in 200 m of water along the south side of St. George Island (169.3°W, 56.3°N) in June 1997 and recovered in April 1998. This mooring contained a bottom-mounted, upward-looking, 150-KHz ADCP. These data permit us to better understand the pattern of flow in the study area.

On each mooring, all instruments sampled at hourly, or shorter, intervals. Most of the data presented in this manuscript were low-pass filtered with a 35 h, cosine-squared, tapered Lanczos filter to remove tidal and higher frequencies, and resampled at 6 h intervals.

Two moorings (P2 and P3) included EnviroTech nitrate monitors (model NAS-2E). The NAS-2E is a syringe-driven (discrete) analyzer that measures nitrate in a similar fashion to the bench-top autoanalyser. Nitrate is reduced to nitrite in a cadmium column, formed into a red azo dye by complexing nitrite with sulfanilamide and N-1-naphthylethylenediamine, and the complexed nitrite is measured colorometrically. Because the instruments do not make separate measurements of nitrite, units reported for the moored instrument are μM nitrate+nitrite (N+N). Seawater samples and calibration standards were analyzed at 6 h intervals. Blanks were analyzed prior to each measurement and consisted of measuring the absorbance of a standard or sample without reagents. Calibration standards for the NAS-2E were prepared according to guidelines provided by Gordon et al. (1993). Working standards were made in low-nutrient seawater (LNSW) with a known nitrate concentration and stabilized by pasteurization at 80 °C for 6 h following Aminot and Kerouel (1998). To verify stability, standards were analyzed before mooring deployment and again after mooring recovery. The moored standards were found to be within 0.2 μM nitrate during the 5–6 month deployments.

2.4. Satellite images

Images of chlorophyll in the region around the Pribilof Islands were created using Modis Aqua level 1A ocean-color files obtained from the Goddard Space Flight Center's ocean color website (http://oceancolor.gsfc.nasa.gov). We used SeaDAS (http://oceancolor.gsfc.nasa.gov/seadas/) to process and map the files, and to flag cloudy pixels. We then used IDL to form composites of cloud-free areas.

2.5. Numerical modeling

The ocean circulation model used here is the Regional Ocean Modeling System (ROMS) (Song and Haidvogel, 1994; Shchepetkin and McWilliams, 1998, 2003). ROMS is based on the free surface, hydrostatic, primitive equations of ocean circulation, using stretched vertical coordinates that span from the ocean floor to the free surface. ROMS has been implemented for spatially nested modeling of the North Pacific; general features of this system are described in Curchitser et al. (2005). The Southeast Bering Sea (SEBS) grid used in the present study covers the southeastern Bering Sea from east of Unimak Island westward to Amukta Pass, and northward to ~59°N with an approximate horizontal resolution of 3 km. There are 30 levels in the stretched vertical dimension. The model is nested within a larger-scale North Eastern Pacific (NEP) model, which has a grid resolution of ~10 km. Initial conditions and boundary values for the SEBS runs are taken from the NEP grid. Both the NEP and SEBS runs are forced by Community Climate System Model (CCSM) atmospheric and large-scale oceanic hindcasts. The tidal runs are forced with tidal parameters provided by Mike Foreman at the Institute of Ocean Sciences (Sidney, British Columbia, Canada). Combined tidal-sub-tidal boundary conditions are based on the algorithms of Flather (1976), Chapman (1985) and Marchesiello et al. (2001).

3. Atmospheric forcing and ice extent: 2004

Winds play a critical role in the dynamics of the Bering Sea shelf. In addition to influencing currents and controlling surface mixing, they largely determine sea-ice production and advection. Mean wind direction at St. Paul Island (1955–present) is out of the north from mid-September through June (Stabeno et al., 1999b). The winds then reverse and are out of the south for the summer. The winds during 2004 deviated from this pattern—they were southerly in April and May, weakly northerly in June, and returned to southerly in August (Fig. 2). From mid-May through early
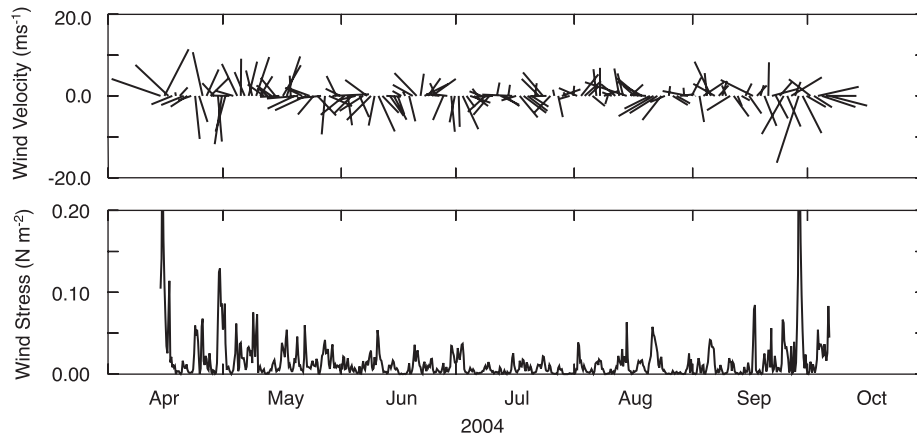
Fig. 2. Daily-averaged wind velocity (top) and wind stress (bottom) measured at Pribilof Island meteorological station. Upward-directed vectors in the top panel indicate winds toward the north.
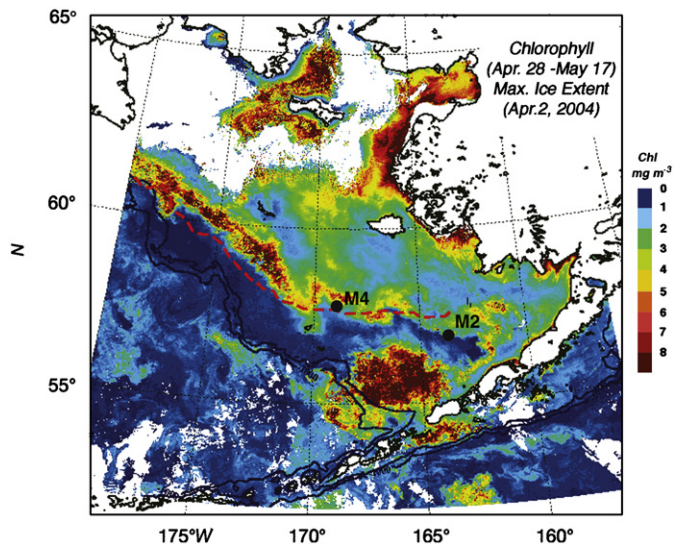
Fig. 3. The maximum extent of ice (50% areal concentration) on April 2 is indicated by the dashed red line. The chlorophyll is composited from all Modis satellite images from April 28 to May 17, 2004. The apparent high chlorophyll along the Alaskan coast north of Nunivak Island is likely a false signal due to sediment contamination. The locations of M2 and M4 are indicated.

Table 2
Monthly averaged salinities at M2 during the last 11 years

Year	Upper water column (<20 m)		Lower water column (>44 m)		Ice presence
	May	July	May	July	
1995	31.6	31.7	32.1	32.1	3/21-4/18
1996	31.7	31.7	31.8	31.7	2/13
1997	31.3	31.3	31.5	31.5	3/10-4/7
1998	32.0		32.0		1/5-2/23
1999	31.7	31.7	31.8	31.8	2/8, 3/1-3/29,5/10
2000	31.9	31.9	31.9	32.0	1/3-1/31
2001	32.1	32.0	32.1	32.1	None
2002	31.9	32.0	31.9	32.0	2/18
2003	31.9	31.8	31.9	31.9	None
2004	32.0	31.9	32.0	32.0	None
2005	32.0	31.9	32.0	32.1	None

September 2004, the winds were relatively weak with only a few storms, and most of those were in August.

The southern Bering Sea is a marginal ice zone during winter and spring. Ice-related processes play a critical role in bottom water formation, fluxes of heat and salt (Coachman, 1986), generation of baroclinic flow in the marginal ice zone (Muench and Schumacher, 1985), and stratification. At higher trophic levels, the spatial patterns of temperature near the bottom of the water column, which are set up by the presence of melting ice in the winter, influence the distributions of fish and shellfish over the eastern shelf (Ohtani and Azumaya, 1995; Wyllie-Echeverria, 1995).

Satellite data of ice extent begin in 1972. The ice extent during 2004 was below long-term average (1972–2006), but was one of the more extensive ice years during the recent warm period (2001–2005), when ice formation and extent were much reduced (Stabeno et al., 2007b). Maximum sea-ice extent in 2004 was a bit south of M4 (Fig. 3), but ice did not reach the Pribilof Islands in substantial concentrations or extend as far south as M2.

Maximum extent occurred in early April (Fig. 3), although there was a similar extent in mid-February (Stabeno et al., 2007b). The ice was then pushed northward by the southerly winds that dominated during April and May (Fig. 2).

Melting sea ice alters underlying water properties in both temperature (colder) and salinity (fresher). The cold air associated with ice advance also cools the water beyond the ice edge (Stabeno et al., 2007b). The lack of sea ice over the southeastern shelf in 2001–2005 resulted in depth-averaged temperatures on the shelf being 2–3 °C warmer than temperatures in the 1990s (Stabeno et al., 2007b). Melting ice also freshens the water column, especially the surface layer. Unlike temperature, however, the immediate impact of ice on salinity is limited to the water beneath the ice.

Ice retreat/melt often occurs when winds are still strong enough to cause substantial vertical mixing. In addition, the frontal structures that divide the shelf into domains often have not formed at the time of ice retreat, permitting substantial cross-shelf advection.

These horizontal and vertical processes smooth the salinity gradients, complicating the relationship between ice extent (or date of ice retreat) and salinity. This complexity is evident at M2, where 12 years of data have been collected. The lowest monthly mean salinity at M2 was observed in 1997, when ice was extensive and persistent (Table 2), and the winds were particularly weak (Stabeno et al., 2001). At M2, years with no ice or an early ice retreat (before March) tended to have higher salinities in

the surface layer than in years with later ice retreat. The exception to this pattern was 1996, when there was little ice and relatively low salinity. Because there was no winter mooring at M2 in 1996, it is difficult to determine the cause of the lower salinity that year. Advection can play a role in modifying the salinity at the mooring site, as was evident in the bottom water in 1995, when the bottom salinity suddenly increased by ~0.4 in April (Stabeno et al., 1998). It is expected that over the outer shelf and in the vicinity of the Pribilof Islands, the impact of local ice melt on the water column is even less persistent than over the middle shelf because of the stronger advection in the region (Stabeno et al., 1999a).

The presence of sea ice also can affect the local timing of the spring phytoplankton bloom. If significant concentrations of sea ice occur after mid-March, an ice-associated phytoplankton bloom usually occurs (Stabeno and Hunt, 2002). This pattern is supported by 12 years of time-series data at M2 and 9 years at M4. Historically, this ice-associated phytoplankton bloom accounts for between 10% and 65% of the total annual primary production (Niebauer et al., 1989, 1995, 1999). During 2004, a well-developed band of high concentrations of chlorophyll was located just within the maximum ice-edge extent in mid-April (Fig. 3). This pattern of higher chlorophyll concentrations persisted for >40 days along this edge (not shown). The band of higher chlorophyll was well north of the Pribilof Islands (M4 was within the band), so sea ice did not play a significant role in determining the timing of the spring phytoplankton bloom in the vicinity of the Pribilof Islands.

4. Currents, temperature and salinity in the vicinity of the Pribilof Islands

4.1. Lagrangian flow

Since 1984, almost 100 satellite-tracked drifters (drogue depth ~40 m) have been deployed or advected into the region around the Pribilof Islands. Following the method in Stabeno and Reed (1994) and Reed and Stabeno (1996), a map of the mean flow at ~40 m was calculated utilizing the trajectories of these drifters (Fig. 4). There were typically between 12 and 25 independent estimates of velocity in each grid cell. Grids with less than four independent estimates are blank. The BSC is evident beyond the shelf break. The anti-cyclonic flows around St. Paul and St. George Islands were largely tidally induced (Kowalik and Stabeno, 1999). Similarly, an anti-cyclonic flow occurred around the island pair. Away from the islands, the flow along the 100-m isobath was relatively broad and weak, although it intensified as the shelf narrows south of St. George Island. The flow then turned northward paralleling the 100-m isobath, with the strongest flow seaward of that isobath. These patterns of flow are supported in part by the front that separates the well-mixed coastal water around the islands from the adjacent, more stratified water (Kinder et al., 1983; Coyle and Cooney, 1993). This frontal structure was particularly evident in 2004 on the eastern side of the islands (Sullivan et al., 2008).

It is evident from Fig. 4 that most of the flow enters the region around the Pribilof Islands from the south. During the last 20 years, more than 50 satellite-tracked drifters have passed through or near Unimak Pass; of these, 29 were advected northward along the 100-m isobath to the Pribilof Islands. More than 70% of those that reached the vicinity east of St. George Island were advected westward via the high-speed flow south of St. George Island. The remaining drifters were transported to the east of the island where they stalled for a period of weeks to months. So, although the majority of the transport along the 100-m isobath flowed westward over the narrow shelf south of St. George Island, it was not uncommon for some weak northward transport to occur east
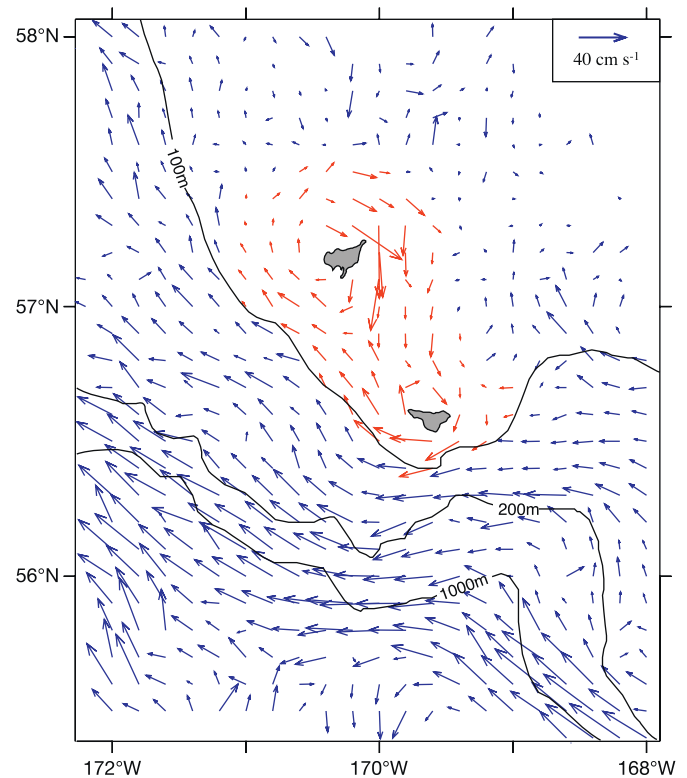
Fig. 4. Mean Lagrangian velocities interpolated to 0.1° latitude × 0.2° longitude. A minimum of four independent estimates of velocity was required to determine velocities in each grid cell. The depth of the drifters' drogues was centered at ~40 m. Red arrows indicate the Pribilof domain.

of the islands. Such flow occurred in fall 2003 and winter 2004 to set up the drifter positions (Fig. 5).

In 2004, there were 20 satellite-tracked drifters that were either deployed in the Pribilof region or were transported into the area from other regions (Fig. 5). While the overall pattern of flow around the islands was similar to the mean (Fig. 4), there was considerable temporal variability. Flow during May and June was relatively weak, especially to the east of the islands. In late July, the flow became more energetic. Two of the drifters that had been advected east of the islands the previous fall and winter, and remained stationary there suddenly moved southward and entered the westward flow to the south of St. George.

4.2. Temporal variability at the mooring sites

While the drifters give a spatial perspective of the general flow at 40 m, data from the series of moorings deployed in the vicinity of the islands provide information on vertical structure, temperature, salinity and temporal variability. The moorings around the Pribilof Islands fall into three groups (Fig. 1; Table 1). Three moorings (P1, P5 and P6) were in shallow water (~60 m); three moorings (P2, P3 and P4) were deployed in deeper water (~100 m); and the remaining two moorings (P7 and P8) were deployed at the shelf break (~180 m) and only measured near-bottom currents, temperature and salinity. In contrast to the moorings around the Pribilof Islands, which were expected to be influenced by waters originating at the shelf break, M2 and M4 on the middle shelf are isolated during the summer months from slope water by the middle transition (Stabeno et al., 2007b).

The time series collected at P7 and P8 captured events of onshelf flux of water from the slope. The salinity (red lines in
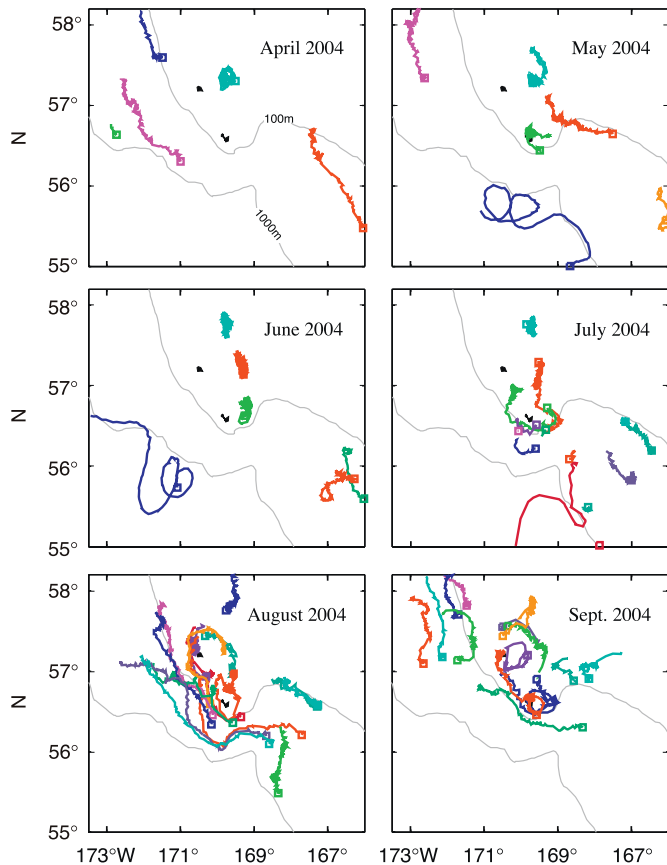
Fig. 5. Monthly trajectories of satellite-tracked drifters that were in the vicinity of the Pribilof Islands in 2004. Squares indicate the position of each drifter at the beginning of the month.

Fig. 6) at these two sites was related to the direction of flow. At P8, when the flow was strongly northeastward (e.g. up-canyon), intrusions of high-salinity water occurred; when the flow was either weak ($<5\,\mathrm{cm\,s^{-1}}$) or had a southward component, the water was less saline. Flow at P7 (situated in the western arm of the canyon) was stronger, both in the mean and in eddy kinetic energy, and more persistent than at P8 (Table 3). While the currents at P8 were relatively weak and interspersed with short periods (days) of strong flow ($\sim20\,\mathrm{cm\,s^{-1}}$), currents at P7 varied on fortnightly scales. At P7, northwestward flow brought more-saline water onto the shelf, while westward flow carried lower-salinity water along the shelf edge. Westward flow was likely water that originated over the outer shelf, while northwestward flow consisted of water that originated in Pribilof Canyon. Thus, Pribilof Canyon was a source of slope water for the region around the Pribilof Islands. This higher salinity water was associated with higher nutrients (see Section 4.3).

At the shallower sites, the near-bottom flow was anti-cyclonic around the islands (Table 3 and Fig. 6). The velocity time series at P1, P3, P4 and P5 contained only short periods (1–3 days) of reversals. The salinity at two of the shallower moorings (P1 and P5) decreased over the deployment period. At the third shallow mooring, P6 (east of St. Paul Island) salinity remained relatively constant, similar to that at the middle shelf domain moorings, M2 and M4 (not shown). In contrast, the near-bottom salinity at the three deeper moorings (P2, P3 and P4) had fairly large excursions of ~0.4 psu with some freshening through September. These large excursions likely resulted from meanders of the middle transition between the Pribilof and outer shelf domains. Meanders in the

transition zone resulted in the moorings at times being within the fresher Pribilof domain and at other times in the more-saline outer shelf domain.

Historically, there have been few oceanographic observations around the Pribilof Islands during the late fall and winter months because of the storminess and the possibility of sea ice. The failure to recover P2 in the fall provided us with some indication of how oceanographic conditions change around the islands during the winter (Fig. 6, bottom panel). While there was considerable variability and some freshening during the summer period, in October, P2 registered a sudden, marked increase in salinity. This persisted at least until late December when a fishing boat dragged the mooring from its site.

A second winter time series is from an ADCP mooring deployed in a water depth of $\sim200\,\mathrm{m}$ south of St. George Island in 1997–1998 (Fig. 7 and Table 3). Although this mooring was deployed for only a single year, data from it show apparent seasonal differences in flow. While it is not reliable to determine an annual cycle from a single year of data, this set of data does support some of the conclusions drawn from the data collected in 2004. Further, winds can be an important forcing mechanism and are markedly seasonal. During summer the flow in the upper water column was stronger and steadier than near the bottom. In late September, however, coincident with the spin-up of fall storms, the strength of currents increased almost two-fold. This is particularly evident at the deeper bins (Fig. 7). The strength of flow was not too different from that observed at P7, although the spin-up in the currents at P7 (October 1, 2004–February 1, 2005) was not as pronounced as occurred in 1997 (Table 3). One explanation for the increase in salinity in October at P2 (Fig. 6) is that fall storms spun up the shelf currents and broke down the summer frontal structure, increasing the amount of slope water introduced to the shelf. The resulting higher salinity persisted until the following spring, when the frontal structures once again became established. This pattern of intrusion of slope water onto the shelf in the fall and winter also occurs at M2 and M4 (Stabeno et al., 2007b).

Five Pribilof moorings successfully collected near-surface data (Fig. 8). At each of these sites, freshening occurred, similar to that observed at the bottom of the two shallower moorings (P1 and P5; Fig. 6). Currents in the upper layer at P1 and P5 increased notably in mid-July (Fig. 8). A weaker response occurred near the bottom at P1 and P5 (Fig. 6). This increase in speed occurred at a similar time to the sudden movement observed in the satellite-tracked drifters (Fig. 5).

There was not enough vertical resolution in the salinity measurements on the moorings to determine vertical structure, but there was enough resolution in the temperature. Temperature data from the moorings (Fig. 9) exhibited three basic patterns of vertical structure—the two-layer structure of the middle shelf (M2 and P6), the weak stratification due to tidal and wind mixing in the Pribilof domain (P1 and P5), and the gradual stratification of the outer shelf (P3 and P4).

Beginning in late April, the water column at each of the sites was thermally well mixed or weakly stratified (Fig. 9). At M2 and P6 (the middle shelf), the surface water warmed while the bottom layer (especially at M2) remained relatively constant. Until mid-July, the mixed-layer depth was shallow ($<12\,\mathrm{m}$ at M2), and it then deepened to $\sim18\,\mathrm{m}$. The mixed layer deepened again in August with the onset of stronger storms. The deepening in mid-July occurred at approximately the same time that the flow around the Pribilof Islands increased, as evidenced by data from the drifters and moorings.

The water-column structure at the two shallower moorings (P1 and P5) was more weakly stratified than over the middle shelf (Fig. 9). At P1, when the flow was westward, middle-shelf water
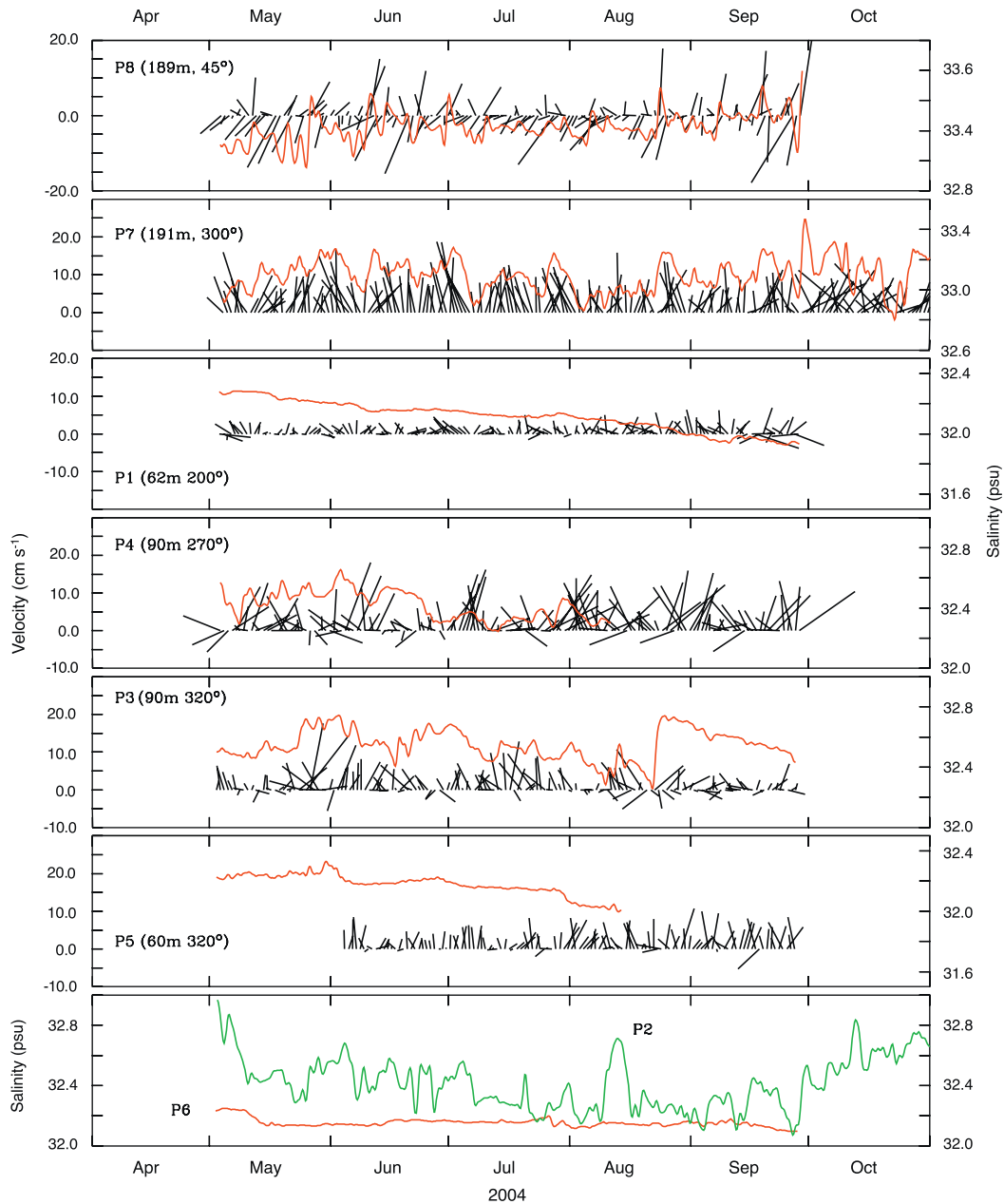
Fig. 6. Near-bottom currents and salinity at the moorings. The depth of each velocity time series is given in parentheses. The depths of salinity instruments are provided in Table 1. The currents were rotated to the along-isobath direction, which is also indicated. The depths of salinity instruments are provided in Table 1.

was transported between the islands. Mixing occurred over the sill between the two islands and to the west of P1, and so, when the tidal currents reversed, the vertical structure was reduced. As expected, P5, which was downstream from P1, was less stratified than P1, because the water had undergone greater mixing. Thus, the bottom layer of the middle-shelf waters was mixed upward into the water column. As we shall see in Section 5, this nutrient-rich bottom layer (Stabeno et al., 2001) provided critical nutrients to support prolonged primary production around the islands.

The water column at P3 and P4 was more typical of outer-domain water (Fig. 9). At the bottom, a well-mixed layer (20–35 m) occurred throughout the deployment period. There were too few observations to resolve the surface-mixed layer, but it was typically less than 20 m deep, except for a short period in August and in later September when strong storms deepened it.

The times series from selected mooring instruments are displayed as a temperature–salinity relationship (Fig. 10), revealing the envelope of the data in *T–S* space. At M2, the water column was relatively cool ($<2\,°C$) and fresh (32.0 psu) in late April, warming and freshening as the summer progressed. The water at P4 was slightly more saline than M2, and P3 was more saline yet. While all the near-surface temperatures warmed by $\sim10\,°C$, the bottom temperatures remained relatively constant at 3–$4\,°C$ in the vicinity of the Pribilof Islands and 2–$3\,°C$ at M2 (44 m is in the bottom layer). The largest range in salinity, not surprisingly, was near the bottom at P7 at the shelf break. There was no trend in salinity at P7, rather the scatter of points indicates the range of temperature and salinity at the slope. In contrast, the surface water at P3 (light green) and P4 (light blue) steadily became fresher, approaching the *T–S* properties that occurred on the middle shelf.

Table 3
Velocity statistics at each of the moorings

Mooring	Bin thickness (m)	Depth (m)	Net speed/direction (cm s^{-1}/°)	Variance* $(\sigma_u^2 + \sigma_v^2)/2$ (cm^2 s^{-2})	Maximum speed (cm s^{-1})
P1		8	4.0/146	574	78
	2	30	3.2/198	530	83
		62	1.9/193	483	62
P3		14	5.2/321	257	81
	4	30	4.9/318	210	52
		62	4.2/314	158	53
		90	2.7/314	149	58
P4		14	6.4/279	350	95
	4	30	6.4/276	342	72
		62	7.1/275	376	65
		90	5.4/274	260	59
P5		8	5.3/318	550	85
	2	30	7.0/327	531	98
		60	3.6/319	266	72
P7		189	8.0/300	245	61
			8.3/296	262	66
P8		186	2.0/281	182	55
St. George		33	8.9/274	289	78
(1997–1998)	4	61	7.7/278	307	78
		101	6.0/289	229	82
		181	5.6/270	242	71

P7 has two values, the top is for the period of April through October 1, and the second is October 1, 2004 through February 1, 2005. Variance* is an indication of the eddy kinetic energy and is the average of the sum of the variance of hourly time series of u and v
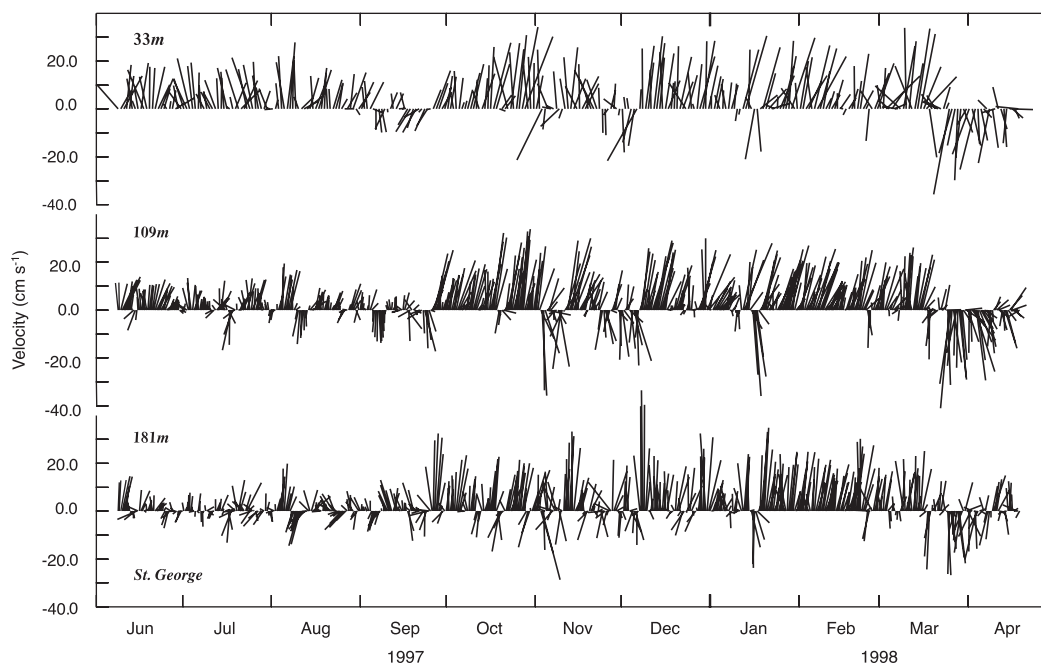
Fig. 7. Low-pass filtered currents measured south of St. George Island (169.33°W, 56.30°N). Currents were rotated 270° so that an upward-directed vector indicates eastward flow.

4.3. Nutrients

More saline water was also typically rich in nutrients (Sullivan et al., 2008; Mordy et al., 2008). To examine the temporal variability of nutrients and their relationship to salinity, nitrate monitors were placed on two of the moorings near the bottom. The meter on P2 was damaged, but the instrument on P3 operated from late spring until mid-summer (Fig. 11, top panel). Through-out the record, there were relatively high concentrations (>17 µM) of nitrate plus nitrite (N+N) at P3, with the highest concentrations occurring in mid to late July. It is evident from the contours of nitrate concentrations collected from the hydrographic survey (Sullivan et al., 2008) that there was considerable spatial variability in the nutrient concentrations, and currents could advect water of different temperature, salinity and nutrient properties. Because the tidal currents were stronger
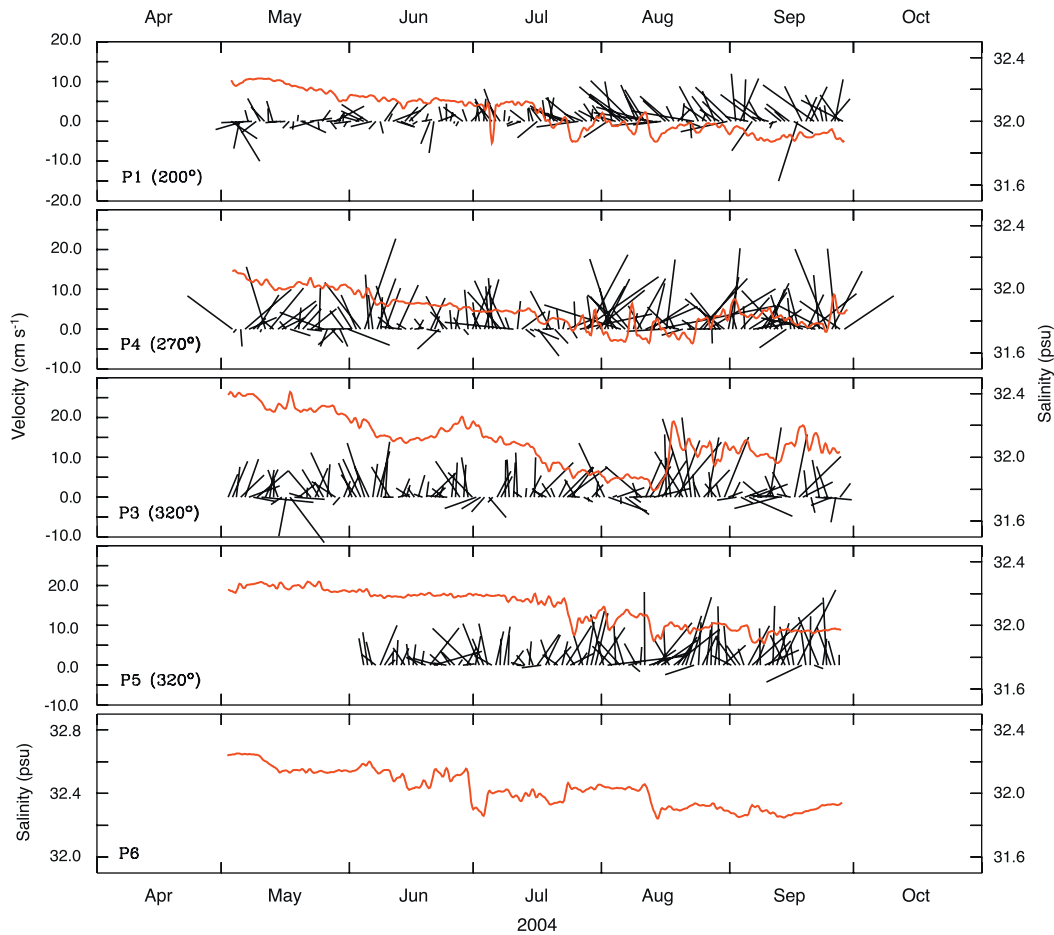
Fig. 8. Daily-averaged velocities and salinity (red) at ~12 m at five Pribilof Island moorings. The currents were rotated to the along-isobath direction indicated in parentheses.

than the low-frequency currents, the semi-diurnal changes in salinity and nutrients stand out in the time series (Fig. 11, bottom panel). When the flow was from the south or southeast, the salinity and the nutrients tended to decrease; when tidal currents were from the opposite direction, the salinity and nutrients increased. In addition to semi-diurnal and diurnal variability, there was also a fortnightly signal in N+N, especially in June and July. During periods of strong tidal variability, tidal swings in N+N were 1–4 μM. The variability of N+N (on diurnal tidal scales) was greatest on July 17–23 when semi-diurnal shifts were as great as 6 μM.

Except for the period of July 11–25, there was a strong correspondence between the salinity and N+N on tidal to weekly scales, as can be seen in both time series (Fig. 11) and for periods of a few weeks in the regression analysis (Fig. 12). From April 29 to May 22, there was little variability in the salinity and N+N time series (Fig. 11), the tidal swings on May 13–15 notwithstanding. On May 23, both salinity and N+N increased for about 2 weeks, and salinities during this period were the highest of the record. Thereafter, there was greater variability of salinity and N+N on tidal to weekly scales, and, except for July, these parameters co-varied. This result was not surprising as N+N is a salt, albeit a non-conservative one.

The data appear to fall into four periods during which there were significant correlations between N+N and salinity (Fig. 12). Despite this correlation between salinity and N+N on smaller time scales, the regression of N+N with salinity for the entire time series was not significant ($r^2 = 0.13$). Instead, regression analysis

demonstrates that the relationship between N+N and salinity was modified during the course of the deployment (Fig. 12). As discussed earlier, spring was apparently dominated by slope water, and fall by 100-m isobath water or even middle-shelf water, as identified by Sullivan et al. (2008). This is consistent with the freshening of the time series from June to August, and overall freshening of the study area during the summer of 2004, as noted above. However, lower N+N concentrations were not associated with this overall freshening, i.e. there was no significant difference in N+N concentrations between the first 30 days of the time series (April 30–May 29, 19.4±0.6 μM) and the last 30 days (July 15–August 13, 21.8±2.1 μM). It is important to note that all of the data from the 2004 cruise fall within the envelope of the historical data in the Bering Sea (not shown).

5. Timing of the spring phytoplankton bloom

Variability in the physical forcing results in considerable interannual variability in the timing of the spring phytoplankton bloom over the eastern shelf, including the Pribilof Islands (Zeeman and Jensen, 1990; Zeeman, 1992). Physical mechanisms that can influence the timing and magnitude of the phytoplankton blooms include onshelf flux of nutrient-rich water, the presence of sea ice, and mixing/onset of stratification (Stabeno et al., 1998, 2001, 2007). There is also spatial variability in the timing and magnitude of the bloom, with the shelf break (the "green belt") having higher primary production than the shelf (Springer et al.,
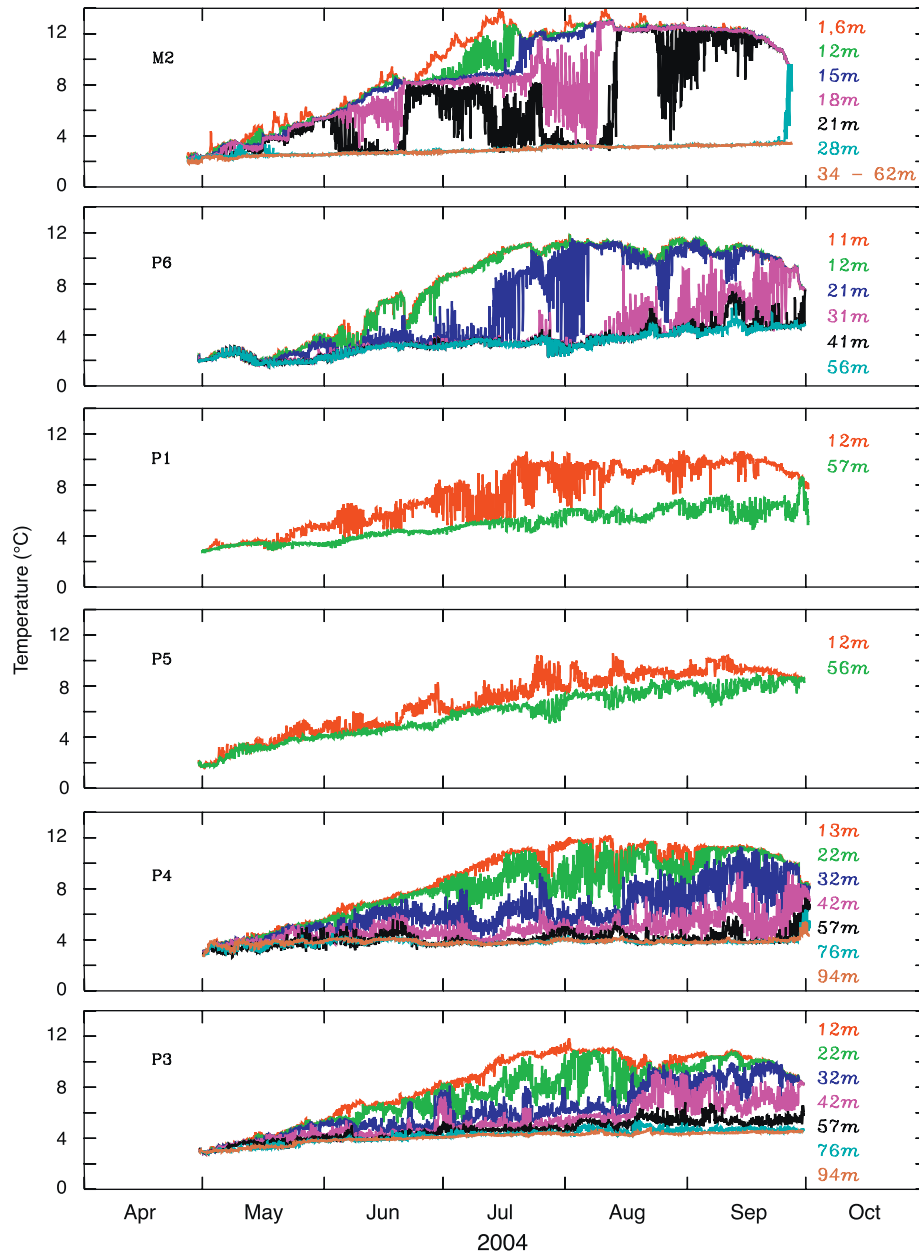
Fig. 9. Hourly temperature from the moorings. The depth of each time series is indicated in each panel. At M2, the time series at 1 and 6 m are plotted in red, and the five time series between 32 and 64 m are all plotted in brown.

1996) and the coastal domain blooming earlier than the middle or outer domains.

Because sea ice did not reach the Pribilof Islands in 2004, an ice-associated bloom was not observed around the islands, although satellite images (top panel Fig. 13) indicate a bloom occurred in late April and early May in the shallower water around St. Paul Island. This region (water depth < 50 m) is comparable to the coastal domain of the Bering Sea. By late May, there were high concentrations of chlorophyll over much of the ocean surrounding the Pribilof Islands (Fig. 13). Unfortunately, clouds and fog limited satellite visibility in summer, but using available images, it is evident that by early July, higher chlorophyll concentrations persisted primarily along the shelf break and between St. Paul and St. George Islands (Fig. 13).

Large eddies that occur regularly along the shelf break south of the Pribilof Islands can influence primary production

(Okkonen et al., 2004). Such influence has been observed along the shelf break in the Gulf of Alaska at similar latitude to the Pribilof Islands (Ladd et al., 2005). Fig. 13 (top two panels) shows the evolution of an eddy just south of the Pribilof Canyon. An eddy dipole formed in early May (55–56°N, 169–172°W), with higher chlorophyll water apparently drawn off the shelf by the anti-cyclonic eddy and advected around the cyclonic eddy. By late May, the cyclonic eddy was gone, and the anti-cyclonic eddy had expanded and moved westward. In 2004, there apparently was not any direct influence by eddies on the primary production in the vicinity of the islands, as the eddy did not intrude into Pribilof Canyon.

The phytoplankton blooms at M2 and at M4 during 2004 were not related to the blooms at the Pribilof Islands. M4 was within the band of high chlorophyll that stretched across the shelf and was associated with the maximum April ice extent (Fig. 3). The

phytoplankton bloom at M2 was delayed and possibly related to the southward migration of the ice-associated phytoplankton bloom—the mean flow at M2 during summer is weakly southward (Stabeno et al., 2007b).

Spatial patterns evident in the satellite images are reflected in the time series of fluorescence at the mooring sites (Fig. 14). It is unfortunate that the fluorometer settings at three of the sites (P1, P3 and P4) were such that the instruments could not resolve the higher magnitudes of fluorescence, but "pegged out". While this caused problems in relating fluorescence to chlorophyll concentrations, it did not hinder discerning the timing of the phytoplankton blooms. The periods of higher fluorescence, and presumably higher chlorophyll, persisted for several weeks, with considerable high-frequency variability. At the northernmost site, M4, the bloom began before deployment of

the moorings, probably sometime in mid-April in association with the presence of sea ice. Elevated fluorescence persisted into June. A similar pattern occurred at P6. In contrast, the bloom began later (mid-May) at M2 and P4 (the two southern moorings). Between the islands (P1), chlorophyll concentrations increased in late May, and persisted into September, except for a short period in late June and early July. This prolonged period of higher fluorescence was likely a result of the vertical mixing by tides of the nutrient-rich bottom water (likely from the middle shelf) into the euphotic zone. Each of these time series also show short periods of higher fluorescence (e.g., late August at M4, P5 and P2, and later September at M2) that appeared to be related to increased wind stress and the associated changes in the mixed-layer depth (Fig. 9).

In contrast, the fluorescence behavior at the two western moorings P3 and P5 was more complex. Both of these moorings had a bloom in the last half of May, likely the spring phytoplankton bloom, but enhanced fluorescence also was observed in July. While the higher fluorescence at P5 may have been associated with the advection of the chlorophyll and/or
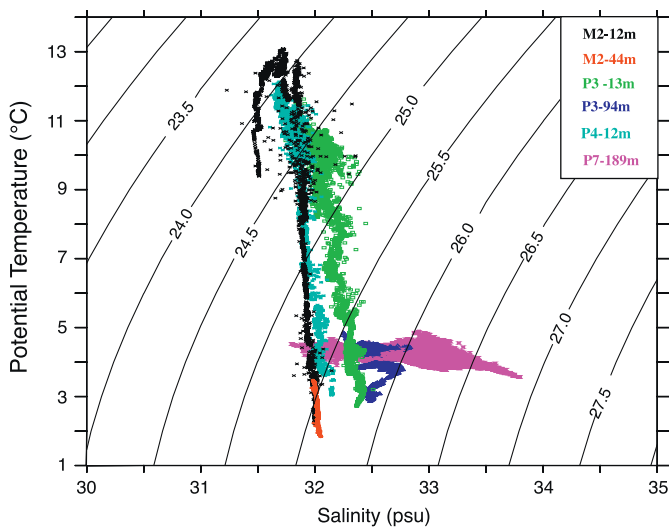
Fig. 10. The T–S relationship of selected time series for April through September at M2, P3, P4 and P7. The depths of the instruments are indicated in the panel in the upper right hand corner. The start of the each time series (except P7) is at its minimum temperature. P7 does not have a trend, and the plot indicates the T–S range that was observed there.
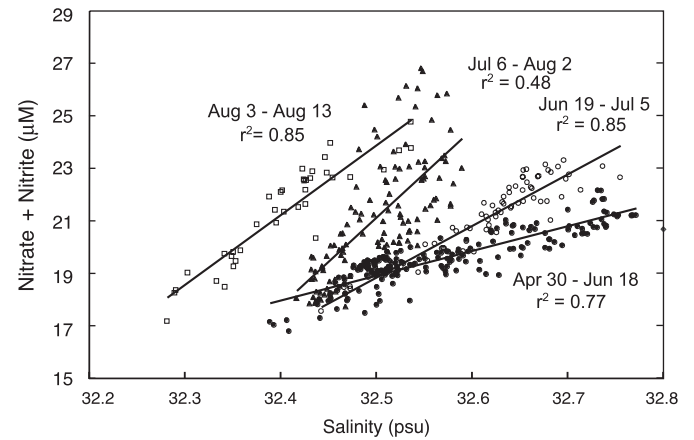
Fig. 12. Relationship between nitrate+nitrite (N+N) at 91 m and salinity at 94 m for four periods during the mooring deployment.
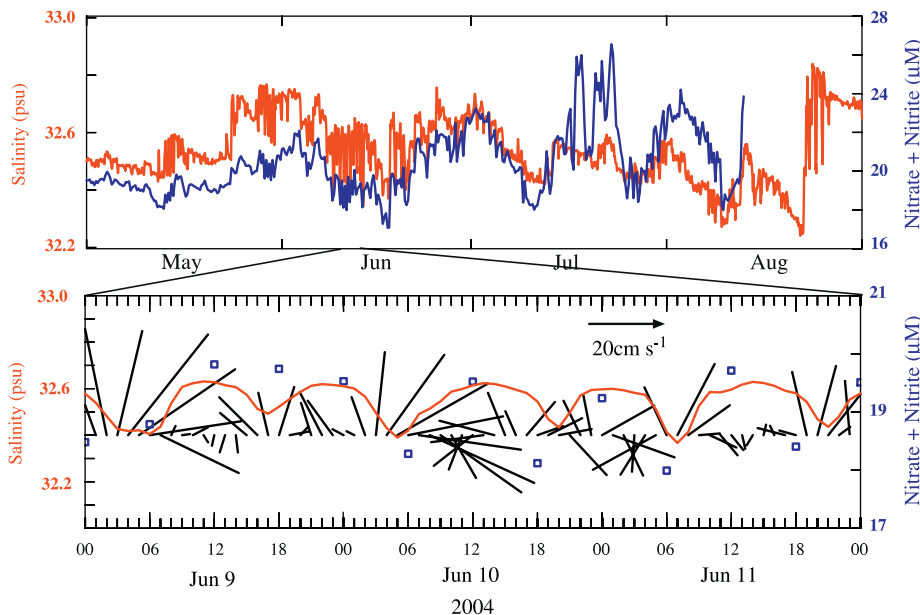
Fig. 11. Nitrate and salinity measured at 91 m at P3. The bottom panel shows the relationship between currents (200 °T), salinity and nutrients for a 3-day period in June.
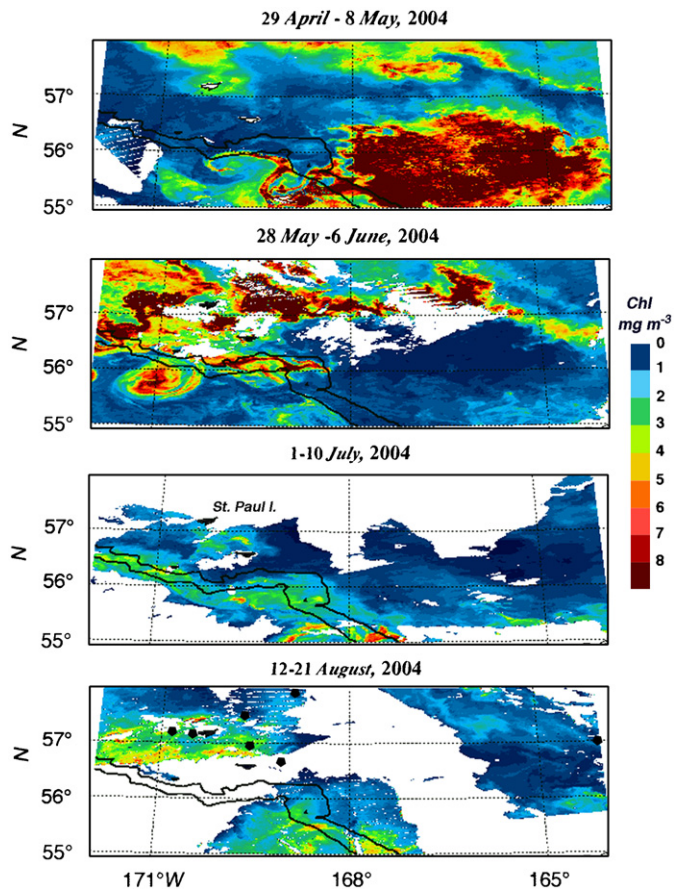
Fig. 13. Ten-day composites of chlorophyll from Modis for the four periods indicated. The locations of all moorings that had a fluorometer at 11 m are indicated by black dots in the bottom panel.

nutrients measured at P1, the increased fluorescence at the deeper P3 mooring does not appear to be related to a comparable signal elsewhere in this array of moorings. The increased fluorescence may have been related to blooms on the outer shelf. For instance in Fig. 13, second panel, a patch of high chlorophyll extends from the shelf break to the area surrounding P3.

6. Numerical model

The Southeast Bering Sea (SEBS) model simulations provide an indication of the mechanisms that control flow and dynamics around the Pribilof Islands. The flow around the islands has a strong tidal component, which also contributes to the sub-tidal, clockwise flow around the island (Kowalik and Stabeno, 1999). The magnitude of the tidal contribution to the low-frequency flow is evident in contours of average (April 1–October 1, 2004) modeled currents on a transect between St. Paul and St. George Islands (Fig. 15). When tides were not incorporated into the model, the average flow between the islands was weak (maximum $<4.5\,\mathrm{cm\,s^{-1}}$). In contrast, when the model forcing included tides, the flow was much stronger in vicinity of both islands. Along the south side of St. Paul Island, the low-frequency currents were as much as 10 times the strength as in the model run without tides. The strength of this flow was similar in magnitude and direction to that measured by satellite-tracked drifters. These results support previous contention that the rectification of tidal currents

is an important source of advection in the vicinity of the Pribilof Islands (Kowalik, 1999; Kowalik and Stabeno, 1999).

The model (when tidal forcing was included) also produced reasonable simulations of the observed temperature structure observed at the moorings. These simulations replicated the two-layer structure and temperature cycle at M2 (Figs. 9 and 16). Without tides, the bottom layer in the model simulation was not well mixed (not shown). Similarly, the observed structure and warming at P4 (over the outer shelf southwest of St. George Island) was replicated in the model simulation. The greatest discrepancy between the model and temperature observations was that the bottom layer warmed more in the model than was observed in the time series. This may be a result of the vertical resolution in the model which is ~2.6 m near the thermocline, which results in a smoothing of the two-layer structure and hence greater vertical mixing.

The data collected at the mooring sites provided a description of an apparent seasonal cycle of salinity in the vicinity of the Pribilof Islands. During fall 2004, with the breakdown of frontal structure, saline, nutrient-rich water was advected onto the shelf and around the islands. This persisted until spring, when the fronts were re-established. The water around the Pribilof Islands then began to freshen. This freshening continued until fall. The fact that this cycle was not unique to 2004 supports the implication of seasonality. Historical salinity data west of the Pribilof Islands can be grouped into two areas: a box to the west of St. George Island (56.4–56.9°N, 171–170°W) and a second box to the west of St. Paul Island (56.9–57.4°N, 172–170.4°W). From 1977 to 2004, 61 stations in nine different years were occupied in the box west of St. George Island and 57 stations in 13 different years were occupied west of St. Paul Island. Virtually all the data were from spring (April–May) or late summer (August–September). At St. George Island, salinity was 32.3 in spring (11 casts) and 31.9 in summer (50 casts). These values were similar to those observed at a depth of 12–14 m on the moorings in 2004. At St. Paul Island, the averaged salinity at 10 m was 32.3 in the spring (seven casts) and 32.0 in the late summer (49 casts).

In the model runs, the overall salinity was ~1 psu too high. This was a result of initiating the temperature and salinity fields of the small-scale model from the larger-scale model runs. Although the absolute salinity was incorrect, the relative temporal changes in salinity were similar to those observed at the mooring sites in 2004. Without tides, the modeled salinity at P4 varied greatly, but did not have a freshening trend (Fig. 17 top panel). In contrast, when the model included tides, there was a freshening of about 0.4 (bottom panel); this freshening was also observed at the mooring site. At the other mooring site, the freshening in the model simulations was less evident.

The model showed the spin-up of the system in early fall that was observed at the moorings (Figs. 6 and 8), including a marked increase in the salinity. What was not evident, however, was the spin-up in July observed in the current meter and drifter data.

7. Discussion and conclusions

The Pribilof Islands sit in close proximity to the middle shelf, outer shelf and slope. The bottom layer of the middle shelf (Stabeno et al., 2007b) and the bottom water from the slope both have high concentrations of nutrients. Water from these sources was mixed by tides and winds, supplying nutrients to support the Pribilof Island's productive marine ecosystem. For instance, in the shallow region between St. Paul and St. George Islands (e.g., P1), vertical mixing continually introduced nutrients to the euphotic zone, supporting a prolonged phytoplankton bloom seen both in
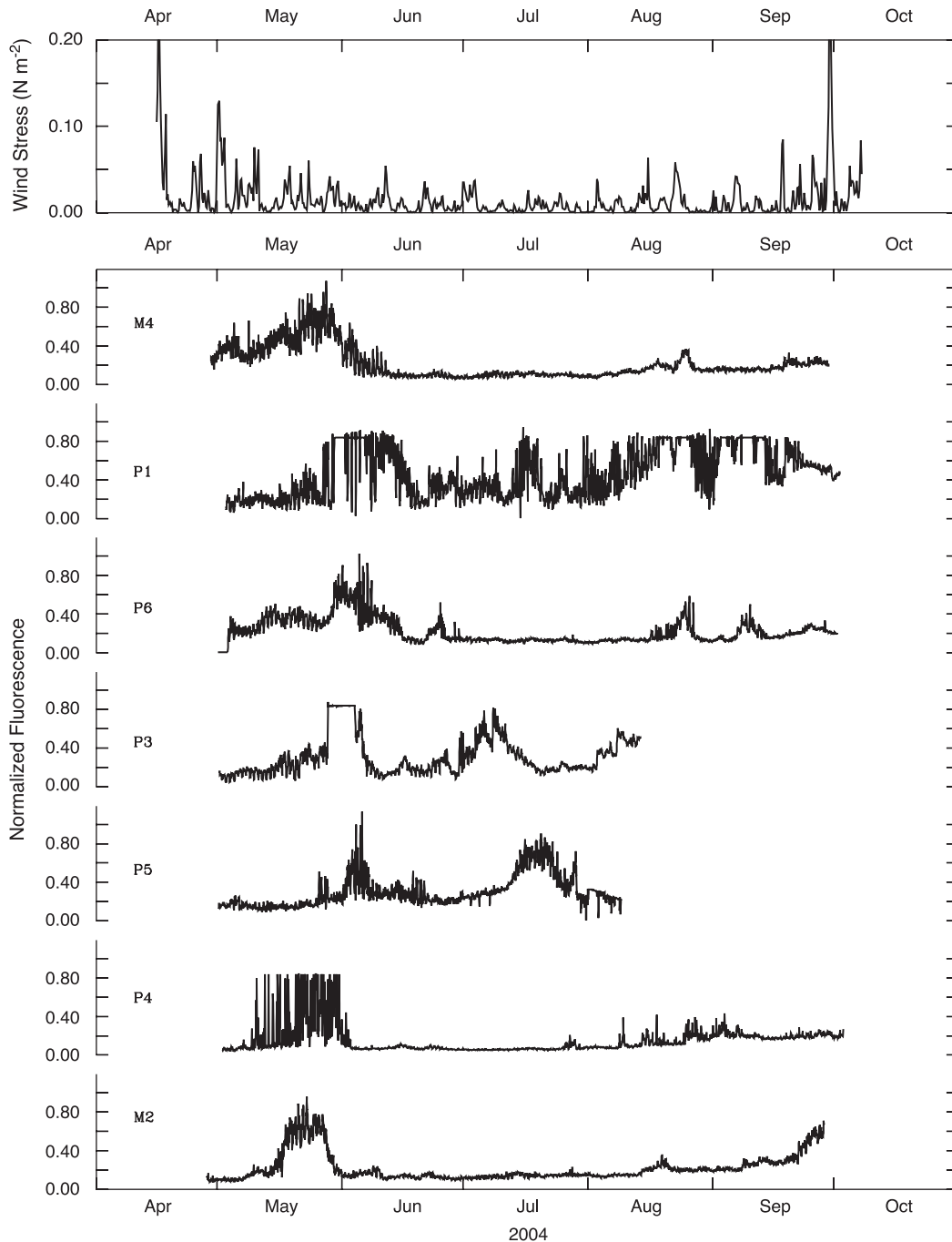
Fig. 14. Time series of wind stress measured at St. Paul Island (upper panel) and normalized fluorescence (hourly) at the each of the mooring sites.

satellite images and time series (Figs. 13 and 14). One source of these nutrients was net westward flow of middle-shelf water between the islands. A second source was the nutrient-rich slope water that was advected onto and along the shelf south of St. George Island. Strong tidal currents between the islands forced some of this water into the region between the islands, especially early in the summer. Vertical mixing between the islands then introduced these nutrients into the surface water. This continual supply of nutrients into the euphotic zone resulted in prolonged production (e.g., mooring sites P1, P3 and P5).

Both observations and model simulations showed freshening during the summer at several of the mooring sites around the Pribilof Islands. There are two possible sources for this less saline

water. The first is the flow of Gulf of Alaska shelf water through Unimak Pass, which is then advected northward along the 100-m isobath. The second is the large reservoir of fresh water over the middle shelf. An estimated transport of $0.3 \times 10^6 \, \mathrm{m^3 \, s^{-1}}$ flows through Unimak Pass (Stabeno et al., 2002). There is a strong seasonal signal in both transport (strongest flow is in the winter) and salinity (it is freshest in January and most saline in the fall). In the past two decades, 29 satellite-tracked drifters have passed through or near Unimak Pass and were advected northward along the 100-m isobath to the Pribilof Islands. Transport from Unimak Pass to just east of St. George Island took anywhere from 20 to 200 days, with an average of 84 days and a median of 100 days. Thus, the water that reached the Pribilof Islands during the summer

probably began its trip in the spring. Spring salinities vary considerably in the vicinity of Unimak Pass, but a reasonable estimate would be ~32 psu, with nitrate ranging from 10 to 16 μM (Stabeno et al., 2002). These salinity concentrations are higher than what was observed in August–September at the mooring

Fig. 15. Cross-section of modeled velocity between St. Paul Island and St. George Island. This shows the speed of the average velocity (April 1–October 1, 2004) for two different model runs. The top panel is a ROMS run with tides and the bottom panel is without tides.

sites. In contrast, the salinities observed at M2 were similar to those observed at the Pribilof Islands in the late summer (Fig. 10). Noting this, it is likely that during summer 2004 the source of the freshening around the islands was the horizontal mixing by the tides of middle-shelf water outward into the middle transition. In fact, noting the spring salinity at Unimak Pass it is likely that the middle shelf is the source of the historical freshening that was observed in the two boxes west of St. George and St. Paul Islands. An examination, however, of the contribution of water from Unimak Pass versus the middle shelf would best be explored with models.

One of the puzzles in 2004 is what happened in mid to late July, when a sudden die-off of sea birds on St. George and St. Paul Islands and a change in the zooplankton communities occurred (Benowitz-Fredericks et al., 2008; Coyle et al., 2008). These events coincided with an increase in the mixed-layer depth over the middle shelf at M2 (Fig. 9), an increase in flow at many of the moorings (e.g., P5 Fig. 8), particularly between the islands, and an increase in variability in the salinity time series. One possible scenario is that the middle shelf domain extended to dominate the area around the Pribilof Islands and strengthened the frontal structure between the oceanic water and the middle-shelf water. The strengthening of these fronts would limit the introduction of oceanic copepods onto the shelf near the islands, which would have been detrimental to feeding by sea birds. The strengthened frontal structure also would support a stronger baroclinic flow along the frontal structure. The July spin-up was not evident in the model runs, indicating that the changes around the Pribilof Islands were probably not a result of changes in winds. One possibility of why the model failed to replicate the July spin-up was that the frontal structure in the model simulations was not as strong as in observations. The lack of strong frontal structure in the model would have resulted in weaker baroclinic flow in the simulations.

The timing of any spin-up around the Pribilof Islands could be critical to the well being of this ecosystem. The warming and decrease in ice that has occurred during the last decade (Stabeno et al., 2007b) could have implications for the frontal structures that form around the islands. The lack of ice would result in more-saline water over the southern shelf, and perhaps a weakening of the frontal structure. Changes in atmospheric forcing, however, could alter the input of water from the Gulf of Alaska that enters the Bering Sea through the Aleutian Passes. While this data set cannot address these questions, it does provide critical information to modelers who might explore these questions.
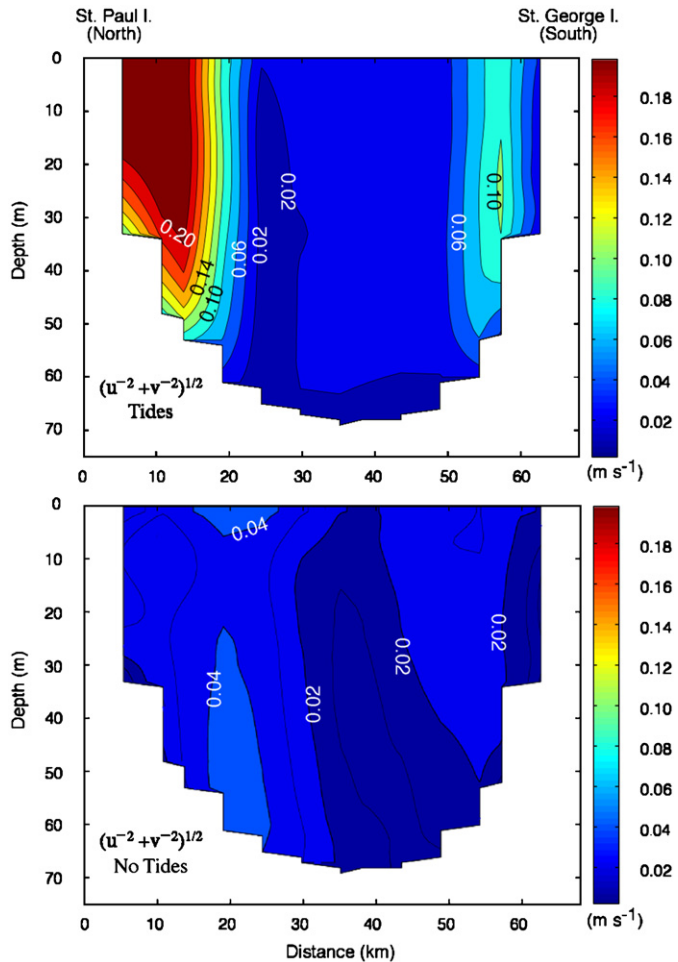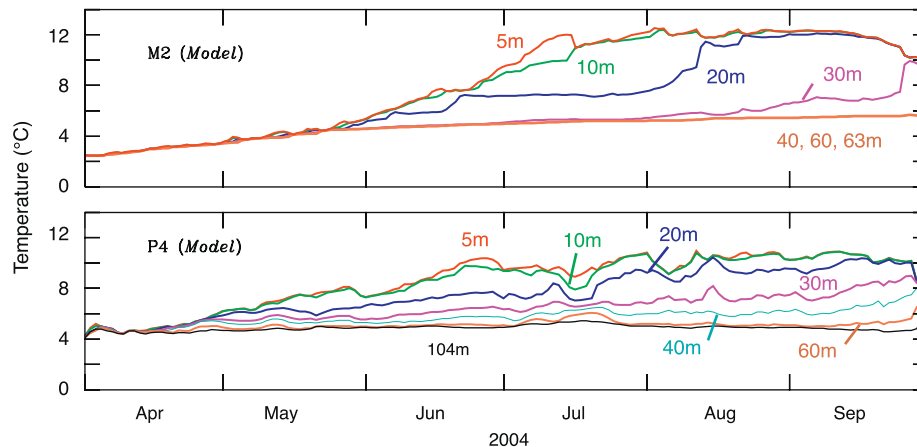
Fig. 16. Temperature at multiple depths from model simulations at M2 (upper panel) and P4 (bottom panel). The model simulation included tides.
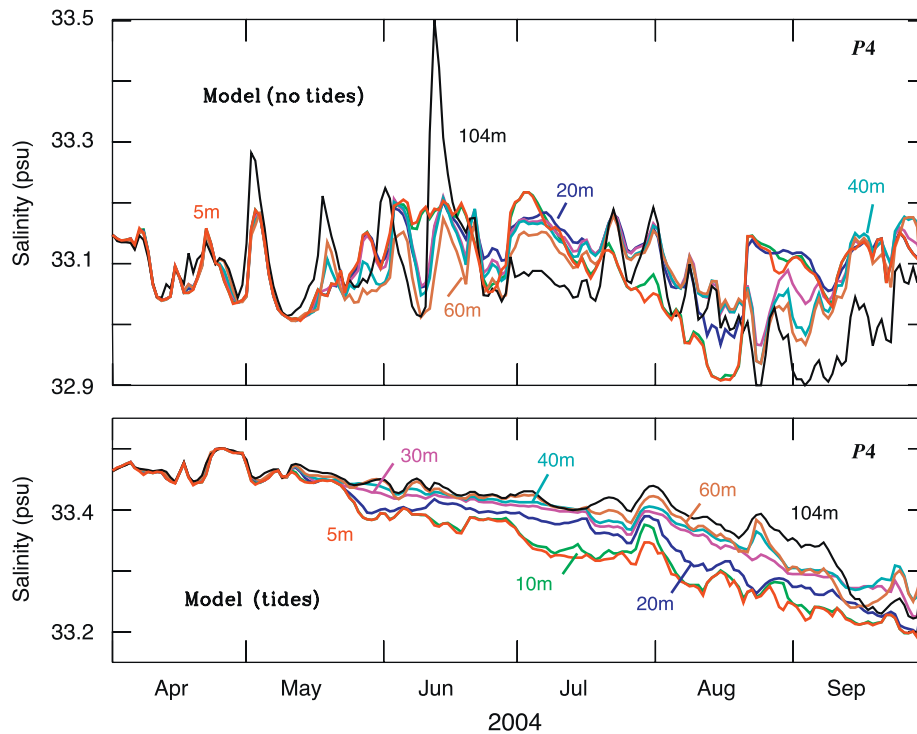
Fig. 17. Salinity at various depths at P4 from model simulations. The model simulation in the top panel had no tidal forcing and in the bottom panel included tidal forcing.

Acknowledgments

References

Aminot, A., Kerouel, R., 1998. Pasteurization as an alternative method for preservation of nitrate and nitrite in seawater samples. Mar. Chem. 61, 203–208.

Benowitz-Fredericks, Z.M., Shultz, M.T., Kitasky, A., 2008. Stress hormones suggest opposite trends of food availability for planktivorous and piscivorous seabirds in two years. Deep-Sea Res. II, this volume [doi:10.1016/j.dsr2.2008.04.007].

Chapman, D.C., 1985. Numerical treatment of cross-shelf open boundaries in a barotropic coastal ocean model. J. Phys. Oceanogr. 15, 1060–1075.

Coachman, L.K., 1986. Circulation, water masses, and fluxes on the southeastern Bering Sea shelf. Cont. Shelf Res. 5, 23–108.

Coyle, K.O., Cooney, R.T., 1993. Water column sound scattering and hydrography around the Pribilof Islands. Cont. Shelf Res. 13, 803–827.

Coyle, K.O., Pinchuk, A.I., Eisner, L., Napp, J.M., 2008. Zooplankton species composition, abundance and biomass on the eastern Bering Sea shelf during summer: the potential role of water column stability and nutrients in structuring the zooplankton community. Deep-Sea Res. II, this volume [doi:10.1016/j.dsr2.2008.04.029].

Curchitser, E.N., Haidvogel, D.B., Hermann, A.J., Dobbins, E.L., Powell, T.M., Kaplan, A., 2005. Multi-scale modeling of the North Pacific Ocean: assessment and analysis of simulated basin-scale variability (1996–2003). J. Geophys. Res. 110, c11021.

Flather, R.A., 1976. A tidal model of the northwest European continental shelf. Mem. Soc. R. Sci. Leige 10, 141–164.

Gordon, L.I., Jennings Jr., J.C., Ross, A.A., Krest, J.M., 1993. A suggested protocol for continuous automated analysis of seawater nutrients (phosphate, nitrate, nitrite and silicic acid) in the WOCE Hydrographic program and the Joint Global Ocean Fluxes Study, WOCE Operations Manual, vol. 3: The Observational Programme, Section 3.2: WOCE Hydrographic Programme, Part 3.1.3: WHP Operations and Methods. WHP Office Report WHPO 91-1; WOCE Report No. 68/91. November, 1994, Revision 1, Woods Hole, MA, USA, 52pp.

Kachel, N.B., Hunt Jr., G.L., Salo, S.A., Schumacher, J.D., Stabeno, P.J., Whitledge, T.E., 2002. Characteristics and variability of the inner front of the southeastern Bering Sea. Deep-Sea Res. II 49 (26), 5889–5909.

Kinder, T., Hunt Jr., G.L., Schneider, D., Schumacher, J.D., 1983. Oceanic fronts around the Pribilof Islands, Alaska: correlations with seabirds. Estuarine, Coastal Shelf Sci. 16, 309–319.

Kowalik, Z., 1999. Bering Sea tides. In: Loughlin, T.R., Ohtani, K. (Eds.), Dynamics of the Bering Sea. University of Alaska Sea Grant, AK-SG-99-03, Fairbanks, AK, pp. 93–127.

Kowalik, Z., Stabeno, P.J., 1999. Trapped motion around the Pribilof Islands in the Bering Sea. J. Geophys. Res. 104 (C11), 25,667–25,684.

Ladd, C., Bond, N.A., 2002. Evaluation of the NCEP/NCAR reanalysis in the NE Pacific and the Bering Sea. J. Geophys. Res. 107 (C10), 3158.

Ladd, C., Kachel, N.B., Mordy, C.W., Stabeno, P.J., 2005. Observations from a Yakutat eddy in the northern Gulf of Alaska. J. Geophys. Res. 110 (C3), C03003.

Marchesiello, P., McWilliams, J.C., Shchepetkin, A., 2001. Open boundary conditions for long-term integration of regional oceanic models. Ocean Model. 3, 1–20.

Mizobata, K., Saitoh, S.-i., Wang, J., 2008. Interannual variability of summer biochemical enhancement in relation to mesoscale eddies at the shelf break in the vicinity of the Pribilof Islands, Bering Sea. Deep-Sea Res. II, this volume [doi:10.1016/j.dsr2.2008.03.002].

Mordy, C.W., Stabeno, P.J., Ladd, C., Zeeman, S.I., Wisegarver, D.P., Salo, S.A., Hunt Jr., G.L., 2005. Nutrients and primary production along the eastern Aleutian Island Archipelago. Fish. Oceanogr. 14 (Suppl. 1), 55–76.

Mordy, C.W., Stabeno, P.J., Righi, D., Menzia, F.A., 2008. Origins of the sub-surface ammonium maximum in the Southeast Bering Sea. Deep-Sea Res. II, this volume [doi:10.1016/j.dsr2.2008.03.005].

Muench, R.D., Schumacher, J.D., 1985. On the Bering Sea ice edge front. J. Geophys. Res. 90 (C2), 3185–3197.

Niebauer, H.J., Day, R.H., 1989. Causes of interannual variability in the sea ice cover of the eastern Bering Sea. GeoJournal 18, 45–59.

Niebauer, H.J., Alexander, V., Henrichs, S.M., 1995. A time-series study of the spring bloom at the Bering Sea ice edge I: physical processes, chlorophyll and nutrient chemistry. Cont. Shelf Res. 15, 1859–1877.

Niebauer, H.J., Bond, N.A., Yakunin, L.P., Plotnikov, V.V., 1999. An update on the climatology and sea ice of the Bering Sea. In: Loughlin, T.R., Ohtani, K. (Eds.), Dynamics of the Bering Sea. University of Alaska Sea Grant, AK-SG-99-03, Fairbanks, AK, pp. 29–59.

Ohtani, K., Azumaya, T., 1995. Influence of interannual changes in ocean conditions on the abundance of walleye pollock (*Theragra chalcogramma*) in the eastern Bering Sea. Can. Spec. Publ. Fish. Aquat. Sci. 121, 87–95.

Okkonen, S.R., Schmidt, G.M., Cokelet, E.D., Stabeno, P.J., 2004. Satellite and hydrographic observations of the Bering Sea "Green Belt". Deep-Sea Res. I 51 (10–11), 1033–1051.

Reed, R.K., Stabeno, P.J., 1996. On the climatological mean circulation over the eastern Bering Sea shelf. Cont. Shelf Res. 16 (10), 1297–1305.

Schumacher, J.D., Stabeno, P.J., 1998. Continental shelf of the Bering Sea. In: Robinson, A.R., Brink, K.H. (Eds.), The Sea, vol. 11. Wiley, pp. 789–822 (Chapter 27).

Shchepetkin, A.F., McWilliams, J.C., 1998. Quasi-monotone advection schemes based on explicit locally adaptive dissipation. Mon. Weather Rev. 126, 1541–1580 http://dx.doi.org/10.1175/1520-0493%281998%29126%3C1541:QMASBO%3E2.0.CO;2.

Shchepetkin, A.F., McWilliams, J.C., 2003. A method for computing horizontal pressure-gradient force in an oceanic model with a nonaligned vertical coordinate. J. Geophys. Res. 108 (C3), 3090.

Song, Y., Haidvogel, D., 1994. A semi-explicit ocean circulation model using a generalized topography-following coordinate system. J. Comput. Phys. 115, 228–244.

Springer, A.M., McRoy, C.P., Flint, M.L., 1996. The Bering Sea Green Belt: shelf edge processes and ecosystem production. Fish. Oceanogr. 5, 205–223.

Stabeno, P.J., Reed, R.K., 1994. Circulation in the Bering Sea basin observed by satellite-tracked drifters: 1986–1993. J. Phys. Oceanogr. 24 (4), 848–854.

Stabeno, P.J., van Meurs, P., 1999. Evidence of episodic on-shelf flow in the southeastern Bering Sea. J. Geophys. Res. 104 (C12), 29,715–29,720.

Stabeno, P.J., Hunt Jr., G.L., 2002. Overview of the Inner Front and Southeast Bering Sea Carrying Capacity programs. Deep-Sea Res. II 49 (26), 6157–6168.

Stabeno, P.J., Schumacher, J.D., Davis, R.F., Napp, J.M., 1998. Under-ice observations of water column temperature, salinity and spring phytoplankton dynamics: eastern Bering Sea shelf. J. Mar. Res. 56 (1), 239–255.

Stabeno, P.J., Schumacher, J.D., Ohtani, K., 1999a. The physical oceanography of the Bering Sea. In: Loughlin, T.R., Ohtani, K. (Eds.), Dynamics of the Bering Sea. University of Alaska Sea Grant, AK-SG-99-03, Fairbanks, AK, pp. 1–28.

Stabeno, P.J., Schumacher, J.D., Salo, S.A., Hunt Jr., G.L., Flint, M., 1999b. Physical environment around the Pribilof Islands. In: Loughlin, T.R., Ohtani, K. (Eds.), Dynamics of the Bering Sea. University of Alaska Sea Grant, AK-SG-99-03, Fairbanks, AK, pp. 193–215.

Stabeno, P.J., Bond, N.A., Kachel, N.B., Salo, S.A., Schumacher, J.D., 2001. On the temporal variability of the physical environment over the southeastern Bering Sea. Fish. Oceanogr. 10 (1), 81–98.

Stabeno, P.J., Reed, R.K., Napp, J.M., 2002. Transport through Unimak Pass, Alaska. Deep-Sea Res. II 49 (26), 5919–5930.

Stabeno, P.J., Kachel, D.G., Kachel, N.B., Sullivan, M.E., 2005. Observations from moorings in the Aleutian Passes: temperature, salinity, and transport. Fish. Oceanogr. 14 (Suppl. 1), 39–54.

Stabeno, P.J., Hunt Jr., G.L., Napp, J.M., Schumacher, J.D., 2006. Physical forcing of ecosystem dynamics on the Bering Sea shelf. In: Robinson, A.R., Brink, K. (Eds.), The Sea, vol. 14B. The Global Coastal Ocean: Interdisciplinary Regional Studies and Syntheses, Harvard University Press (Chapter 30).

Stabeno, P.J., Bond, N.A., Salo, S.A., 2007b. On the recent warming of the southeastern Bering Sea shelf. Deep-Sea Res. II 54 (23–26), 2599–2618.

Stabeno, P.J., Ladd, C., Reed, R.K., 2007a. Observations of the Aleutian North Slope Current, Bering Sea, 1996–2001. Prog. Oceanogr., submitted for publication.

Sullivan, M., Mordy, C., Kachel, N.B., Stabeno, P.J., 2008. The Pribilof Islands: temperature, salinity and nutrients during summer 2004. Deep-Sea Res. II, this volume [doi:10.1016/j.dsr2.2008.03.004].

Whitledge, T.E., Malloy, S.C., Patton, C.J., Wirich, C.D., 1981. A Manual for Nutrient Analyses in Seawater. Formal Report No. BNL 51398. Brookhaven National Laborotory, Upton, NY, 216pp.

Wyllie-Echeverria, T., 1995. Seasonal sea ice, the cold pool and gadid distribution on the Bering Sea shelf. Ph.D. Thesis, University of Alaska Fairbanks, Fairbanks, AK, 281pp.

Zeeman, S.I., 1992. The importance of primary production and CO_2. In: Nagl, P.A. (Ed.), Results of the Third Joint US-USSR Bering and Chuckchi Seas Expedition (BERPAC), Summer 1989. US Fish and Wildlife Service, Washington, DC, pp. 218–224.

Zeeman, S.I., Jensen, P.R., 1990. Photoresponses of phytoplankton in the Bering Sea. In: Roscigno, P.F. (Ed.), Results of the Second Joint US-USSR Bering Sea Expedition, Summer 1984. US Fish and Wildlife Service, Washington, DC, pp. 87–96.